

Article

Performance of Low-Height Railway Noise Barriers with Porous Materials

João Lázaro ^{1,*}, Matheus Pereira ^{1,†}, Pedro Alves Costa ^{1,†} and Luís Godinho ^{2,†}

¹ CONSTRUCT, Faculty of Engineering (FEUP), University of Porto, Rua Dr. Roberto Frias, 4200-465 Porto, Portugal; matheus.pereira@eac.ufsm.br (M.P.); pmbcosta@reit.up.pt (P.A.C.)

² ISE, Department of Civil Engineering, University of Coimbra, Pólo II, Rua Luís Reis Santos, 3030-788 Coimbra, Portugal; lgodinho@dec.uc.pt

* Correspondence: jlazaro@fe.up.pt

† These authors contributed equally to this work.

Abstract: Rail transport is the most sustainable transportation mode, with the lowest energy consumption and carbon footprint. However, the noise induced by railway traffic in urban regions is a significant drawback and several reports point out the risks and the amount of people suffering from direct exposure to railway noise. One of the most used mitigation measures for railway noise is the implementation of noise barriers. Although they offer a significant reduction in noise levels, their height makes people feel enclosed. Therefore, in the case of railway infrastructure, the solution to the problem may lie in the use of barriers with a lower height placed close to the railway track. As the noise-forming mechanisms are mainly located at the track level, placing the barrier in a position close to the track allows mitigating rail noise without causing the problems identified above for the population in the vicinity. The purpose of this paper is to illustrate the development of a barrier solution to be used in a railway context through numerical modelling with the Boundary Element Method (BEM). The solutions developed were placed close to the track and have a low height. The geometry was defined so as to direct the energy back to the track to take advantage of the acoustic properties of the ballast. The addition of a porous granular material on the inner face of the barrier allows the control of reflections between the vehicle body and the barrier, increasing its acoustic efficiency. Finally, considering the most efficient solution, the insertion loss in a network of receivers located 10 m away from the track is analysed in order to study the noise reduction levels in a place where human receivers are usually located.

Keywords: railway noise; low height noise barriers; acoustic efficiency; noise mitigation



Citation: Lázaro, J.; Pereira, M.; Costa, P.A.; Godinho, L. Performance of Low-Height Railway Noise Barriers with Porous Materials. *Appl. Sci.* **2022**, *12*, 2960. <https://doi.org/10.3390/app12062960>

Academic Editor: Massimo Garai

Received: 4 February 2022

Accepted: 3 March 2022

Published: 14 March 2022

Publisher's Note: MDPI stays neutral with regard to jurisdictional claims in published maps and institutional affiliations.



Copyright: © 2022 by the authors. Licensee MDPI, Basel, Switzerland. This article is an open access article distributed under the terms and conditions of the Creative Commons Attribution (CC BY) license (<https://creativecommons.org/licenses/by/4.0/>).

1. Introduction

Railway transport is the most sustainable mode of transport, with the lowest energy consumption and carbon footprint compared to any other mode of transport. However, a report by the European Environment Agency (EEA) [1] from 2019 on this subject states that at the European level, rail noise is the second most dominant source, with an estimated 22 million people exposed to at least 55 dB during the day and night periods. On the same subject, however, with a different time horizon, the report by the European Environment Agency [2], whose aim is to project scenarios for the decade 2020 to 2030, states that the situation of the population's exposure to environmental noise level in Europe will worsen in practically all areas responsible for current exposure levels. The projections suggest that in 10 years more than one million people will be exposed to excessive rail noise, both in urban centres and outside these agglomerations. In light of the above, a report of the World Health Organisation (WHO) Regional Office for Europe [3] is presented. This document highlights the effects of noise and incorporates a number of indications for certain policies that must be implemented in order to ensure health and well-being for people living with the most diverse forms of environmental noise. The WHO working group state

that, for the daytime period, noise levels should be below 54 dB, and for the night-time period, they should not exceed 44 dB. Finally, it stresses that interventions to reduce noise levels and to comply with the limits indicated should focus on interventions at the track level, the improvement of rolling stock and the implementation of small noise barriers.

Rail noise mitigation measures can be applied in three different locations and according to the environment and the level of noise pressure reduction that one wants to achieve [4]. Usually, the most widely deployed solutions are those that act at the level of the propagation path or at the level of the receivers. In places where housing density is high, the solutions that act on the path of propagation are more advantageous in economic terms [4]. Acoustic barriers are usually artificial and solid elements made of different types of material and placed in different positions, depending on the place to be protected. This noise mitigation solution has been widely adopted in the context of road noise mitigation, and there are several methods for designing these solutions. Acoustic barriers can have different operating principles depending on the material they are made of; i.e., they can work by reflecting acoustic waves and/or absorbing them. In general, the barriers are vertical elements between 3 m and 4 m high positioned along the road or railway.

However, despite the inherent benefits of reducing noise and improving the quality of life of the population living nearby, this type of solution faces the reluctance of the populations living near the railway infrastructure. This situation is related to the size of the barrier, affecting the field of vision, causing a sense of imprisonment, loss of natural light or affecting air circulation. From another perspective, for those who travel on trains, complaints are also registered for similar reasons [5–7]. In order to tackle some of the negative points identified for the higher acoustic barriers, namely, being obstacles to one's field of vision, the natural evolution of thinking has led to the creation of solutions whose working principle is similar to the one intended to be applied in the work presented in this document. The inherent advantage of low-height solutions is related to the positioning of this element. As the mechanisms of noise generation are mostly at the level of the rail [8], the placement of the barrier in a position close to the track allows the propagation of sound waves to be interrupted close to the source. The reduced height of these elements thus allows this positioning close to the source without constituting an obstacle to the field of vision of passengers and passers-by.

Bearing this in mind, several authors have worked on this issue in order to develop a solution to mitigate the noise levels associated with rail traffic. The studies from the literature present solutions for the design of the barriers and for a more effective numerical modelling. Koussa [9] studied, both numerically and experimentally, the use of gabion walls as a form of mitigation. The results indicate that this solution can achieve up to 8 dB(A) of insertion loss. Jilibois [10] presents a full-scale model of an L-shaped barrier built with wooden panels and inside with absorbent fibrous material. Tests carried out by the experimental author revealed an attenuation of 10 dB(A). Nieuwenhuizen [11] showed that the Dutch calculation scheme for conventional barriers is reasonably applicable for low-height solutions. Finally, Kasess [12] proposes corrective functions that allow one to efficiently calculate complex geometries using BEM, in order to apply more complex geometries in noise mapping programs. To control the reflections between the car body and the noise barrier, an absorptive treatment is required. Fibers and foams are commonly used in passive noise control; however, for external applications, these materials require protection against environmental agents and structural reinforcement. Because of these requirements, the interest in sound absorptive solutions, such as porous concrete, made using consolidated lightweight and sustainable granular materials have increased over recent decades [13–21]. The investigation of the fluid-equivalent representation of porous concrete made with expanded clay has been shown to be relevant in the scientific community. Carbajo et al. [22] studied perforated concrete and highlighted the higher durability and the excellent strength-to-weight ratio of this solution. Pereira et al. [23] studied the influence of the water–cement ratio, the expanded clay grain size, and the sample thickness in the sound absorption behaviour, while Zolanvari [24] studied the fluid-equivalent representation of porous concrete using different aggregates.

The modelling of the railway scenario has, for the reasons given, an important role to play in forecasting and creating measures to mitigate rail traffic-induced noise. The Boundary Element Method (BEM) is widely used to solve acoustic problems [7,25], and can be an excellent option to model the effect of mitigation measures. The versatility of this numerical method allows the creation of simply reflective acoustic barriers and/or the inclusion of porous material which acts as a sound absorption element, allowing the improvement of the performance on the barrier, mitigating the energy reflected between the vehicle and the barrier. In this article, the BEM will be used to solve an external acoustic problem, essentially to test the geometry of the barriers. In addition, a BEM formulation considering multiple material regions is implemented to allow the modelling of the effect of possible absorptive materials coupled to the noise barrier. Using this model, it becomes possible to model the absorptive materials using equivalent fluid theories, leading to a realistic representation of such media. To assess the capacity of the barrier, the insertion loss was used, i.e., the difference between the scenario with and without the barrier. Using the insertion loss allows the barrier to be assessed as a noise control measure placed in a location with specific characteristics. In this way, the IL calculation presents the actual losses over a wide range of frequencies, for any set of receivers, regardless of the scenario to be evaluated and mainly regardless of the type of material and geometry of the prototype.

This paper's structure is as follows: Section 2 shows the experimental railway noise characterisation. Section 3 presents the experimental procedure used to characterise porous concrete samples, allowing the fluid-equivalent theory representation. Section 4 presents the numerical formulation of the BEM used to model the described problem. Section 5 presents the strategy used to define the barrier's geometry and the parametric study of different noise barrier configurations. Then, Section 6 shows the sound pressure levels predicted around the noise barrier, in the presence of the train, and the insertion loss results. Finally, Section 7 summarises the main conclusions of this work.

2. Railway Noise Characterisation

Noise induced by rail traffic has several sources with different characteristics. Despite the various components of railway noise, the noise generated by the wheel-rail interaction plays the most important role in noise generation. The variable that most conditions the sound pressure levels and the origin of the noise is the running speed of the vehicles as illustrated in Figure 1, where the main noise sources are defined according to the train speed.

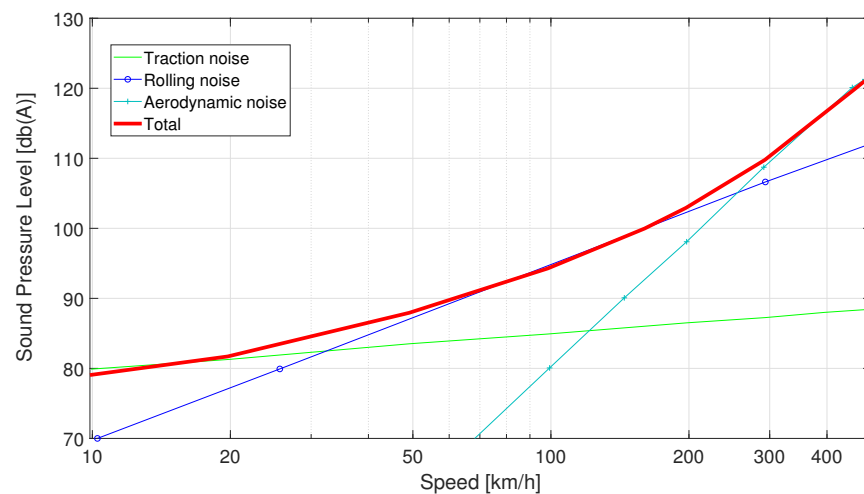


Figure 1. Evolution of the contribution of the different sources according to the speed of circulation (adapted from [26]).

The complete study of the railway noise problem involves examining several dimensions, namely generation, propagation and reception. Therefore, the definition of measures

aimed at its mitigation requires a clear understanding of these dimensions. Consequently, it can be concluded that only the characterisation of noise in different types of scenarios, with different running speeds, vehicle types, track types and urban meshes allows a clearer view of the noise levels involved and especially which variations are associated with the different traffic conditions mentioned above.

In this context, the main objective of the experimental characterisation is to clarify the noise levels associated with the traffic under analysis. The systematisation of maximum noise levels, as well as the frequency content involved, relating them to specific conditions, makes it possible to better define mitigation measures to deal with the noise content identified.

In this work, a characterisation campaign has been performed, in which the acquisition of the signal was made using four microphones Behringer type ECM 8000, connected to a Focusrite Sclarett 4Pre USB for the signal acquisition, as is shown in Figure 2. Post-processing of the data was performed in Matlab using the ITA-Toolbox functions [27].

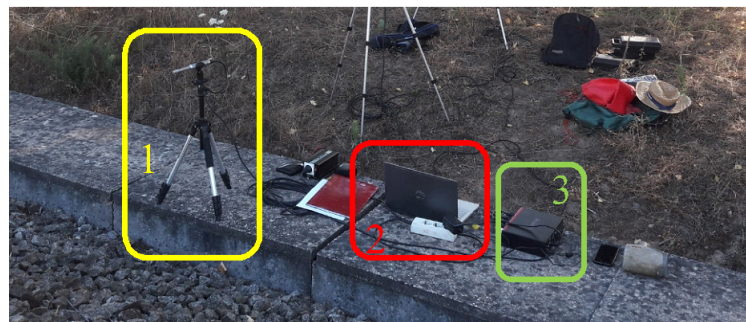


Figure 2. Experimental setup for the acoustic signal acquisition; (1) Behringer ECM 8000 microphone, (2) computer, (3) Focusrite Sclarett 4Pre USB acquisition unit.

The placement of the microphones was defined to allow acquiring the noise in the closest possible place to the source, and at successively larger distances from the source, thus allowing to study in a complete way the propagation of the sound waves. Figure 3 shows the setup used for the measurement, with the distance between microphones and position relative to the track. Figure 4 shows photos taken at the measurement site, in scenarios with and without vehicle, respectively. As can be seen from the illustrations, the microphone called M1 is very close to the source, while the others, M2, M3 and M4, occupy a relative position in accordance with places where pedestrians circulate. Before each measurement campaign, verification was performed making use of a BK 4231 microphone calibrator. Since some of the microphones are positioned close to the railway, some influence of potential air-flow generated by the train passage will inevitably be included in the registered responses. However, the registered acoustic signals are still relevant to better understand the acoustic responses at positions close to the railway, since sound pressure levels at such positions greatly helps to define effective mitigation measures to tackle the exposure of pedestrians and sensible receivers.

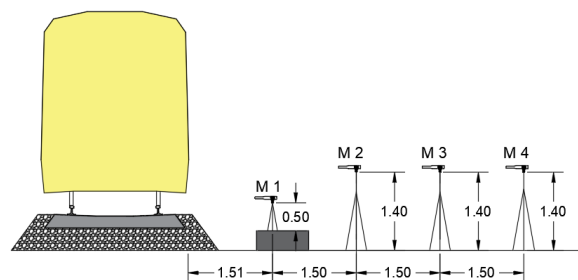


Figure 3. Experimental setup configuration.



Figure 4. Photographs of the in situ experimental characterisation. (a) Photograph of the microphones on site. (b) Photograph of the measurement setup in the presence of the vehicle.

The sound pressure levels (SPL) collected in a ballast track context in each of the four available microphones are shown below, in Figure 5. From the experimental characterisation it was possible to collect data from numerous passages with different running speeds. In order to summarise the data collected, the noise levels corresponding to the two recorded speed (respectively, 84 km/h and 78 km/h) recorded are presented. The data are presented in one-third octave bands and it is intended to highlight from among the various receivers the most significant spectral content that will serve as a basis for the numerical simulations explained in the previous sections.

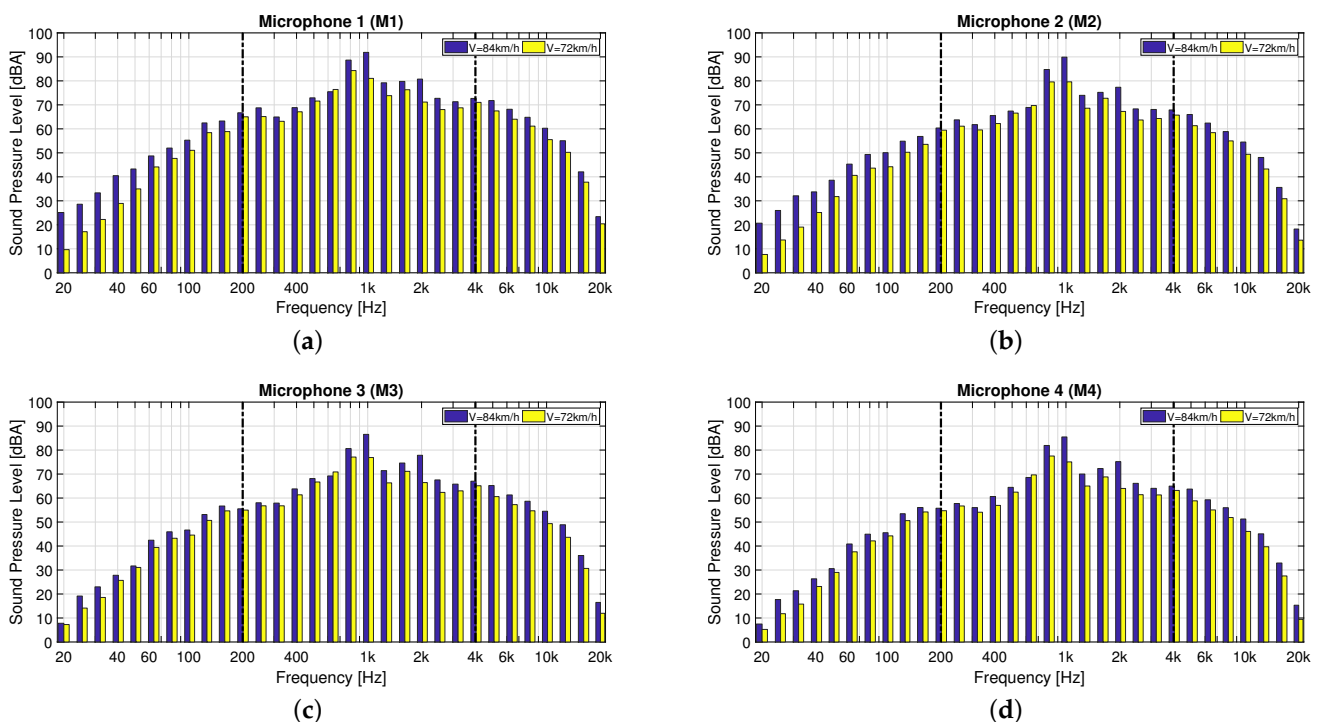


Figure 5. Records of measured sound pressure levels; in blue a vehicle operating at 84 km/h; in yellow a vehicle operating at 72 km/h. (a) First microphone; (b) Second microphone; (c) Third microphone; (d) Fourth microphone.

Sound pressure levels (SPL), presented in Figure 5 are filtered to take into account the response of the human ear, and thus are presented in dB(A). By analysing the one-third octave bands presented, it is concluded that the most prevalent frequency content responsible for the highest noise levels is between 200 Hz and 4000 Hz, i.e., the frequency interval between the two discontinuous black lines in each of the third octave bands. This information has been the basis for the numerical modelling presented later in this paper,

allowing the definition of the frequency range and content that needs to be mitigated by the noise barrier.

3. Experimental Characterisation of Porous Concrete

In the porous concrete material, granules are usually distributed differently from the what is observed in fibrous materials by following a log-normal pore distribution, resulting in smaller porosity and higher tortuosity. The absorption coefficient of these materials depends on the size of the pores, the porosity, the tortuosity and the thickness of the material sample.

Six samples of porous concrete were produced using expanded clay aggregates, with grain size of 0–2 mm. All samples were prepared with 10.1 cm of diameter and thickness of 4, 6 and 8 cm, being these procedure previously presented in [23]. The sample proportions in weight (kg) are presented in Table 1.

Table 1. Materials proportions in weight (kg) of the produced samples.

| Grain Size (mm) | Aggregate (%) | Cement (%) | Water (%) |
|-----------------|---------------|------------|-----------|
| 0–2 | 43.96 | 37.36 | 18.68 |

Several approaches can be used to characterise acoustic absorbing materials, such as those described for example in Ciaburro et al. [28], Arenas et al. [29] or del Rey et al. [30]. Here, an experimental procedure based on the use of an impedance tube was used to characterise the normal incidence acoustic properties of the porous concrete samples. As described in ISO 10534-2 [31], these properties can be obtained from the transfer function between two microphones. To obtain the intrinsic acoustic properties of the porous concrete samples, the Two-Cavity Method proposed by Utsuno et al. [32] was used.

The impedance tube used has a circular cross-section of 10.1 cm diameter, the cut-off frequency being approximately 1600 Hz for the chosen microphone spacing. A white noise signal was used to excite the speaker from the analyser, OR 34 Compact Analyzer, the sound pressure was measured using two microphones B&K Type 4188 1/2", positioned at 16 cm and 10 cm from the sample surface, and the pressure data were post-processed in Matlab, to obtain both the surface impedance and the sound absorption. A schematic representation of the experimental setup is presented in Figure 6, where the term d_1 is the sample thickness, and D is the air cavity thickness.

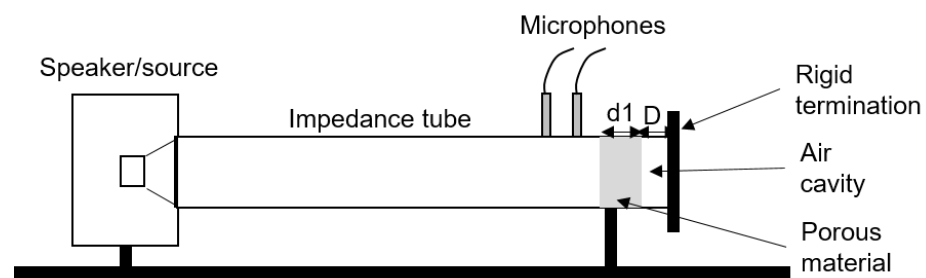


Figure 6. Schematical representation of the experimental two-cavity method (retrieved from [23]).

The two-cavity method is based on two measurements of the same sample through the ISO 10534-2 procedure. Each measurement uses a different air cavity depth, D , between the sample and the rigid termination. The complex characteristic impedance, \tilde{Z}_c , and the complex wave number, \tilde{k}_c , can be determined, respectively, by the following equations,

$$\tilde{Z}_c = \sqrt{\frac{\tilde{Z}_{s1}\tilde{Z}_{s2}(Z_1 - Z'_1) - Z_1Z'_1(\tilde{Z}_{s1}\tilde{Z}_{s2})}{(Z_1 - Z'_1) - (\tilde{Z}_{s1}\tilde{Z}_{s2})}}, \quad (1)$$

$$\tilde{k}_c = \frac{j}{2d_1} \ln \left(\frac{\tilde{Z}_{s1} + \tilde{Z}_c}{\tilde{Z}_{s1} - \tilde{Z}_c} \tilde{Z}_{s2} + \tilde{Z}_c \right), \tag{2}$$

where d_1 is the sample thickness, \tilde{Z}_{s1} is the complex surface impedance measured with the first air cavity depth D , and \tilde{Z}_{s2} is the complex surface impedance measured with the second air cavity depth D' . Z_1 and Z'_1 denote the acoustic impedance of each air cavity,

$$Z_1 = -j\rho_0c_0 \cot(k_0D), \tag{3}$$

$$Z'_1 = -j\rho_0c_0 \cot(k_0D'). \tag{4}$$

The measurements were performed for a rigid termination and an air cavity depth $D = 2$ cm. This option preserves the method's validity and allows minimising the number of measurements for each sample to determine both its sound absorption coefficient and its intrinsic acoustic properties. Figure 7 shows the porous concrete samples and sound absorption curves between samples with different thicknesses. Each curve corresponds to the average between the two samples of same thickness, respectively, 4, 6 and 8 cm. It was observed that the increase in the thickness produces a shift in the sound absorption coefficient curve towards low frequencies.

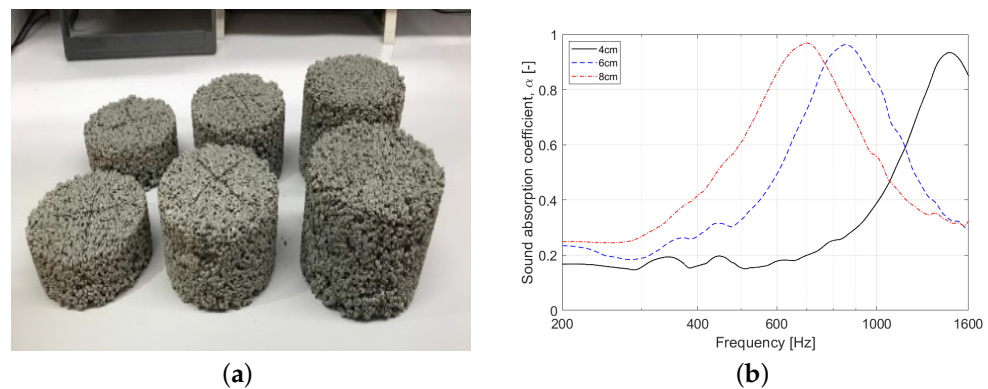


Figure 7. Sound absorption behaviour of porous concrete. (a) Porous concrete built samples. (b) Average of the sound absorption coefficient for three different thicknesses: 4, 6, and 8 cm. (retrieved from [23]).

To predict the acoustic behaviour of porous concrete with different thicknesses and to represent these materials as the fluid-equivalent theory, the Horoshenkov and Swift model was used [33]. This model was derived assuming rigid frame granular media with a log-normal pore size distribution to predict the the characteristic impedance, \tilde{Z}_c , and the wave number, \tilde{k}_c , of porous concrete samples. It considers four macroscopic parameters to determine the acoustic behaviour: air flow resistivity, σ , open porosity, ϕ , tortuosity, τ , and the standard deviation of the pore size, σ_p .

The inverse technique was performed using a genetic algorithm in which the objective function was based on the quadratic sum of errors between the analytical and experimental data, along a frequency range with nf discrete frequency values,

$$OF(\omega) = \sum_{i=1}^{nf} |\alpha_{ana} - \alpha_{exp}|, \tag{5}$$

where α_{ana} is the absorption coefficient obtained from the Horoshenkov and Swift model [33], and α_{exp} is the experimental absorption coefficient. These four macroscopic parameters were previously obtained in [23], and are presented in Table 2. The open

porosity was the only macroscopic parameter experimentally determined, using the water saturation method.

Table 2. Macroscopic parameters obtained for the porous concrete studied samples.

| Airflow Resistivity σ [Ns/m ⁴] | Open Porosity ϕ [-] | Tortuosity α_∞ [-] | Standard Deviation of the Pore Size σ_p [-] |
|--|--------------------------|--------------------------------|--|
| 3896.06 | 0.46 | 1.89 | 0.25 |

Figure 8 shows a comparison between the complex properties using the presented macroscopic parameters and those experimentally obtained through the two-cavity method for a sample with 4 cm. As observed in [34], an excellent agreement can be observed between the experimental data and the semi-phenomenological prediction, allowing us to represent and predict the porous concrete behaviour for different samples thicknesses and geometries.

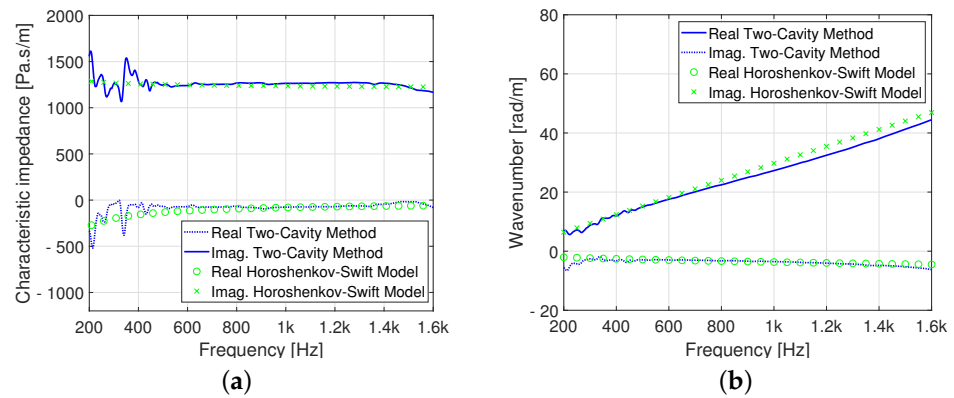


Figure 8. Comparison between the experimental characterisation and the semi-phenomenological representation n . (a) Characteristic impedance, \tilde{Z}_c . (b) Wave number, \tilde{k}_c (retrieved from [34]).

4. Numerical Modelling

The Boundary Element Method, BEM, was used to model the acoustic problem since it allows analysing complex geometries without the need to describe the whole propagation medium, and allows us to solve problems with both infinite or limited domains [6].

In the frequency domain, the problem is governed by the Helmholtz equation,

$$\nabla^2 p + k^2 p = \delta(r_1 - r_0). \tag{6}$$

where p is the acoustic pressure and k is the wave number.

The development of Equation (6) yields Equation (7), which allows the acoustic problem to be solved by integration along the defined boundaries. Thus, solving Equation (7) can be defined as approximating the solutions for each boundary element j .

$$\sum_{j=1}^N v(x, \vec{n}) \int_{\Gamma} i\rho\omega G(x, x_0) d\Gamma_j + \sum_{j=1}^N p(x) \int_{\Gamma} H(x, x_0, \vec{n}) d\Gamma_j + c_p p(x_0) = p_{inc}(x_0, x_f) \tag{7}$$

Usually, the matrix formulation is used as the preferred means to carry out the Boundary Element Method [35,36],

$$\mathbf{C}p - \mathbf{H}p = i\rho_0\omega\mathbf{G}v + p_{inc}. \tag{8}$$

where p and v are the acoustic quantities to be calculated—the pressure and velocity of particles according to the surface—and p_{inc} is the acoustic pressure in the free field due to a source located on the domain. The \mathbf{G} and \mathbf{H} matrices are fully populated matrices. Finally, \mathbf{C} is a diagonal array whose values depend on the collocation point. It is common to add the matrix \mathbf{C} and \mathbf{H} , writing the previous equation in its most simplified form,

$$\mathbf{H}\mathbf{p} = i\rho_0\omega\mathbf{G}\mathbf{v} + p_{inc} \tag{9}$$

The formulation presented up to this point only allows the study of the interaction of the boundaries with a single external medium, in this case, the acoustic medium. In order to represent the porous materials that are to be placed on the barrier and that will be studied in this document, it is necessary to extend the method to include the simulation of porous materials as fluid-equivalents. In other words, it is necessary to simulate more than one propagation medium, with different properties.

Therefore, it is necessary to define each of the media and ensure that in the interfaces between them there is coupling between the pressures and normal velocity.

The systematisation of this problem involves the definition of the equations presented in Equation (7) for each propagation domain and the boundaries valid for both the external, $\Omega_{exterior}$ and internal domain, Ω_i , as illustrated in Figure 9.

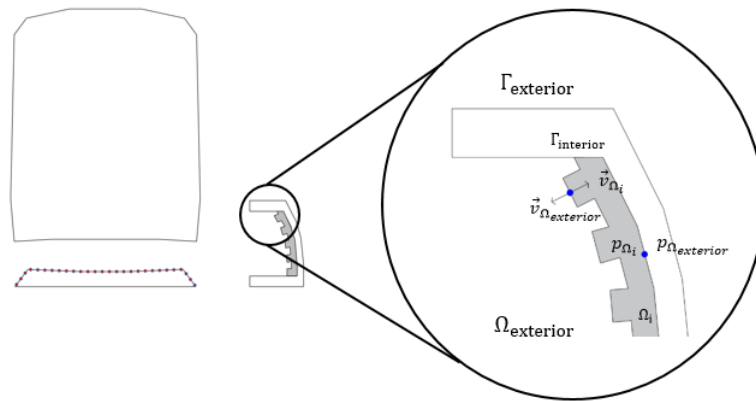


Figure 9. Representation of the coupled interior/exterior problem.

The coupling between domains is achieved by ensuring equilibrium and continuity conditions at the shared boundaries of the domains [37].

$$p_{\Omega_{ext}} = p_{\Omega_{int}} \tag{10}$$

$$\frac{1}{i\omega\rho_{\Omega_{ext}}} \frac{\partial p_{\Omega_{ext}}}{\partial n} = -\frac{1}{i\omega\rho_{\Omega_n}} \frac{\partial p_{\Omega_{int}}}{\partial n} \tag{11}$$

The calculation process involves solving a system of equations taking into account the equations defined for the two mediums under consideration (Equation (7)). The system of equations can be expressed as

$$\begin{cases} i\omega\rho_{\Omega_{ext}}\mathbf{G}_{\Omega_{ext}}\{\tilde{v}\} + \mathbf{H}_{\Omega_{ext}}\{\tilde{p}\} = \{p_{inc}\}, & \text{for air} \\ -i\omega\tilde{\rho}_{\Omega_j}\mathbf{G}_{\Omega_j}\{\tilde{v}\} + \mathbf{H}_{\Omega_j}\{\tilde{p}\} = 0, & \text{for porous material} \end{cases} \tag{12}$$

Once the acoustic variables at the defined boundaries are known, the acoustic pressure at the external receivers is equal to the sum of the incident acoustic pressure and the acoustic pressure resulting from the interaction of the boundaries with the acoustic medium, as shown in Equation (13).

$$p^T = p_{inc} + p^S \tag{13}$$

where p^T is the total acoustic field at the external points, p_{inc} is the acoustic pressure for the free field and p^S is the acoustic field at the external points due the presence of the boundaries.

5. Methodology

The following section describes the methodology used for the design of a low-height acoustic barrier for use in a railway environment. It presents the steps required to define the properties of the boundaries under analysis, the location of the receptors for a better evaluation of the acoustic performance of the solutions, the definition of the barrier geometry and the incorporation of porous material in order to increase its effectiveness. Figure 10 presents a schematic diagram of the steps developed in each section until the final result.

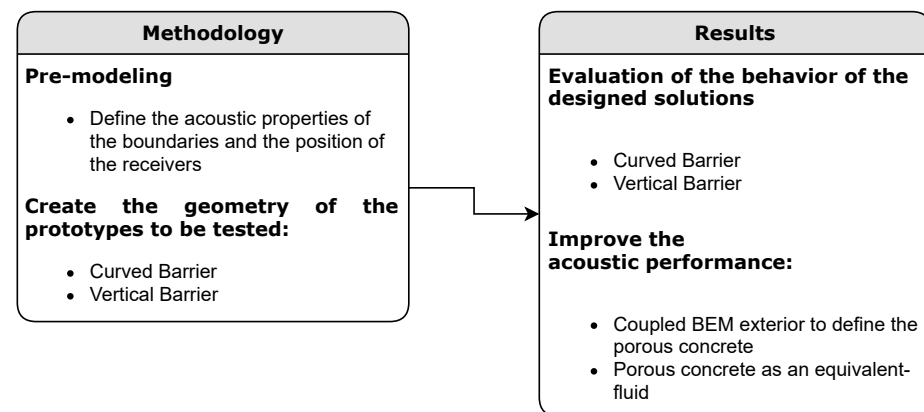


Figure 10. Schematic representation of the methodology and results.

The application of the 2D BEM model makes it possible to analyse how the presence of barriers next to the railway affects the propagation of sound waves.

The adequate discretisation of the boundaries involved in the calculation is an essential step in the application of the numerical method. Figure 11 shows as an example the boundaries considered in the calculation, highlighting for a simple geometry the barrier description, represented by the midpoints of each boundary element. At this stage it is necessary to define the boundary conditions of the elements that are part of the acoustic medium only, which allows us to calculate the system of equations. Except for the porous material, which was defined by the coupling of the external and internal BEM, the other boundaries in contact with the acoustic medium have prescribed boundary conditions. For the vehicle and part of the acoustic barrier, a purely reflective condition was defined, meaning that the particle velocity along these boundaries is null. However, for the track (indicated in the figure as red dots), an impedance condition was prescribed, which allows the ballast acoustic absorption coefficient to be considered.

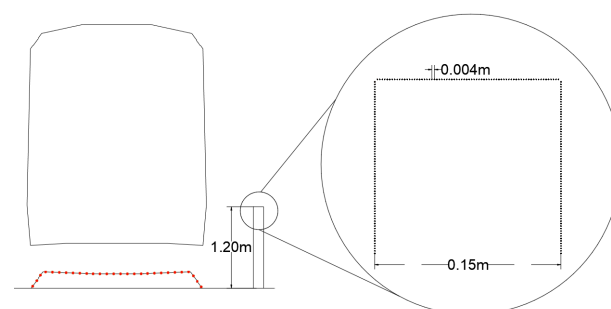


Figure 11. Boundaries to be described and the respective mesh of boundary elements.

Information gathered from Metro do Porto, SA, enabled the modelling of the elements that are part of the railway context, thus being as close as possible to the real scenario.

This information allowed to set the distance between the track and the barrier, based on safety requirements related to track works. Considering this information, the distance between the external rail of the track and barrier was set at 1.225 m. To allow a better performance of the system, a curved barrier was subsequently defined in such a way that the reflection of the incident waves took place in the normal direction to its surface, thus sending more energy back to the origin and taking advantage of the sound-absorbing characteristics of the track. For that purpose, the time domain propagation of an acoustic wave was analysed, in order to better understand the shape of the incident wave front reaching the barrier, and trying to match the inner shape of the barrier to the shape of this wave. Figure 12a presents the time domain simulation of the acoustic wave at the location where the barrier is to be placed, also representing a curved low-height noise barrier with the inner face coinciding with the wave front. The final geometry of the barrier is shown in Figure 12b.

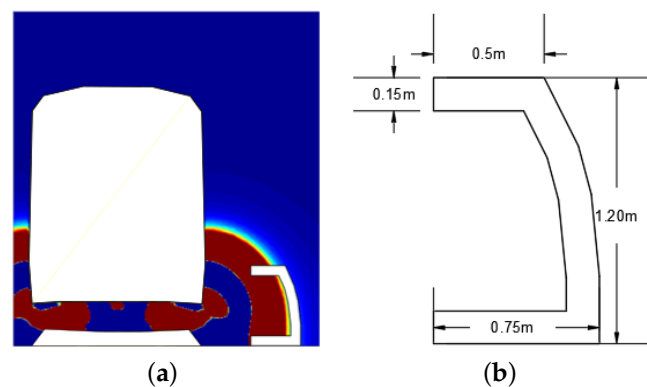


Figure 12. (a) Schematic representation of the wave front and the designed barrier; (b) representation of the main dimensions of the final barrier.

In addition to the considerations described above, it was also necessary to take into account the absorption capacity of the ballast, since the development of the work presented here is based on the premise of an integrated barrier solution. Thus, the development of the barrier geometry sought to take advantage of the acoustic absorption properties of the railway track (ballast). Taking into account the results presented by Broadbent [38] for the acoustic absorption coefficient for a 17 cm ballast layer, the surface impedance was calculated by Equation (14). Figure 13 shows the absorption curve for the diffuse field and the corresponding calculated surface impedance approximation for the calculated frequency range.

This equation originates a real impedance value that is applied to the ballast elements,

$$Z_s = \rho c \frac{1 + \sqrt{1 - \bar{\alpha}}}{1 - \sqrt{1 - \bar{\alpha}}} \quad (14)$$

where ρ is the density of the air, c is the acoustic wave propagation velocity in air and $\bar{\alpha}$ is the absorption coefficient. Finally, receiver points were defined so as to allow the acoustic performance of the noise barrier to be assessed. Their position was defined considering the circulation of pedestrians alongside the track (in the case of the lower receivers) and sensible buildings (in the case of the higher receivers). Figure 14 presents the mesh of the external receivers (black points) used in the studies presented in the following sections. As can be seen, the mesh extends to about 7 m in length and 5 m in height, incorporating the receivers mentioned above.

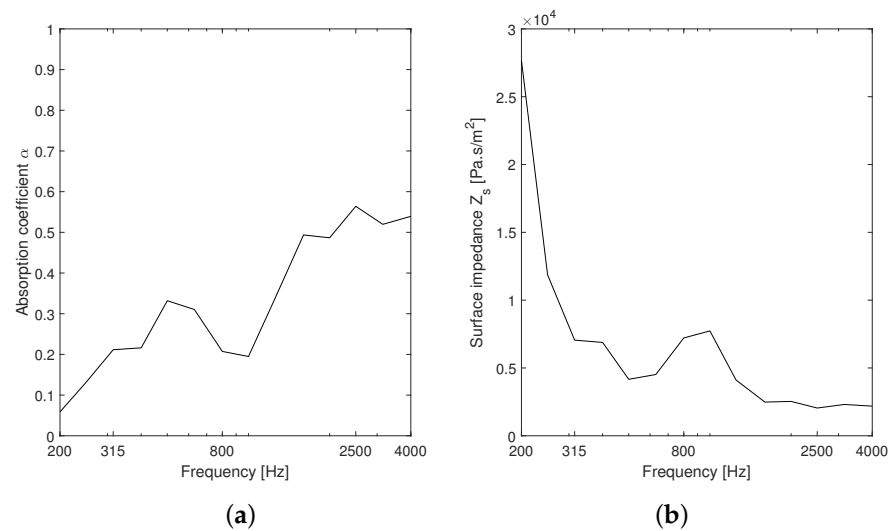


Figure 13. (a) Measured absorption coefficient in the diffuse field (adapted from [38]); (b) corresponding surface impedance used in the calculation model.

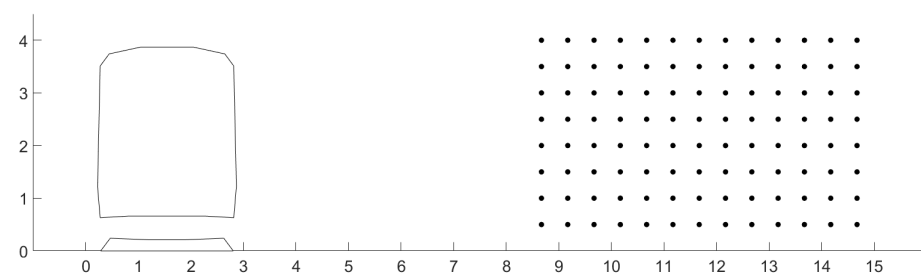


Figure 14. Representation of the receiver mesh used in the simulations.

6. Results

Initially, the acoustic performance of a purely reflective vertical barrier 1.20 m high and 0.15 m thick was evaluated. In Figure 15, we present the sound pressure levels for the scenarios with and without a barrier (see Figure 15a–f), and the respective Insertion Loss (see Figure 15g–i, for three different frequencies: 500 Hz, 2000 Hz and 4000 Hz. From the analysis of the figure, it was found that there are relevant differences between the scenario without a barrier (see Figure 15a–c) and the scenario with a barrier (see Figure 15d–f), meaning that the barrier prevents part of the energy from propagating. This phenomenon is even more remarkable when analysing the insertion loss (see Figure 15g–i), where it was observed that the reduction (warmer colours of the figures) is higher than 15 dB.

The second phase of the parametric study is to analyse the proposed curved geometry. The proposed shape was analysed using the BEM model, and its performance was compared with that of the vertical barrier. In Figure 16, the results computed for the new barrier shape are illustrated. This figure is divided into three parts, illustrating the propagation in the case without a barrier in Figure 16a–c, the scenario with the presence of a barrier in Figure 16d–f, and finally the insertion loss in Figure 16g–i. In the case of the curved barrier, the attenuation effect is very clear, with reductions of over 15 dB. Compared to the vertical barrier (see Figure 15) the insertion loss presented by the curved barrier (see Figure 16g–i), is higher. The phenomenon is once again observed in the warmer colours which make up the insertion loss colour map of the barrier under analysis. The use of the track as a means of mitigation plays an important role in this case, since part of the performance improvement is due to the characteristics of the ballast that absorbs energy sent by the reflection of waves on the inner surface of the curved barrier.

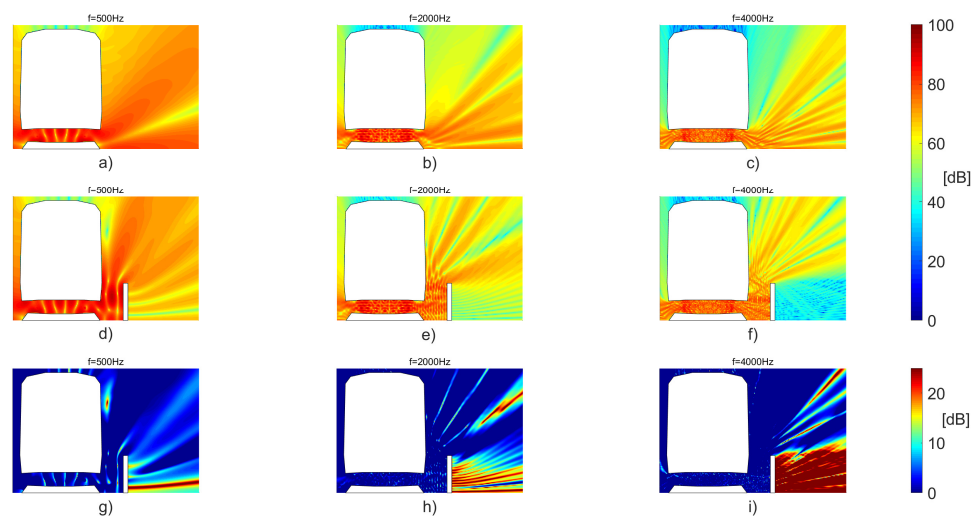


Figure 15. Sound pressure level calculated without (a–c) and with (d–f) the noise barrier and the insertion loss (g–i).

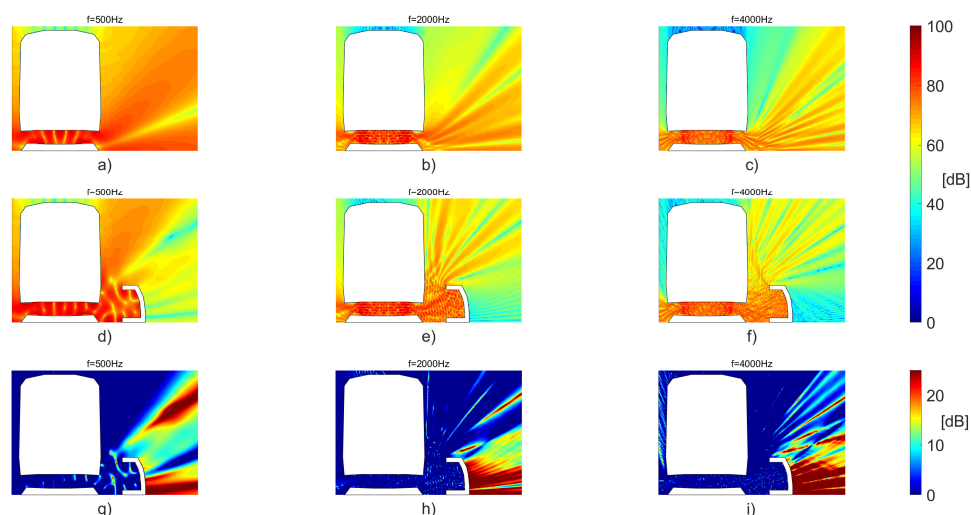


Figure 16. Comparison of the sound pressure levels in the cases without (a–c) and with the barrier (d–f) and the respective insertion loss, first, second, and third rows (g–i).

From the analysis of the geometries of the barriers, it is concluded that the curved barrier is visibly better in reducing the levels of sound pressure in the proximity of the noise source compared to the vertical barrier. However, secondary reflections such as those that occur between the barrier and the vehicle do not suffer significant attenuation and part of the energy is sent back to the external receivers. Thus, an absorptive treatment in the internal face of the barrier is required to reduce the SPL between the train body, the track and the acoustic barrier. As mentioned above, the placement of material with sound absorption characteristics in the barriers guarantees an improvement in acoustic performance, in particular concerning the reflection of sound waves between the body of the vehicle and the body of the barrier.

For this purpose, porous concrete was chosen because of the higher durability and excellent properties for external application, without the requirement of protection against environmental agents and structural reinforcement. Figure 17 shows the geometry of the curved barrier filled by porous material, with an irregular geometry, to increase the absorptive

surface. The geometry of the porous material presented is composed of two parts, namely a regular layer with a thickness of 0.08 m and an irregular layer. The irregular layer is composed of elements 0.06 m thick and 0.10 m wide with equal spacing between them.

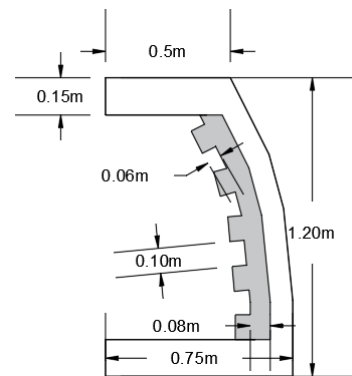


Figure 17. Illustration of barrier geometry and porous material.

Figure 18 shows the insertion loss calculated at the receivers illustrated in Figure 14. For this purpose, the energetic average of the sound pressure in the receivers was calculated for the cases with and without a barrier and the insertion loss was then computed. In what concerns reflective barriers, the analysis shown in Figure 18 corroborates what was already observed in the proximity of the noise source. The curved barrier presents a substantially better performance than the vertical one, particularly from the frequency 630 Hz on. From 200 Hz up to 630 Hz, the insertion loss varies and the vertical barrier is slightly superior at some frequencies. From 630 Hz onwards, the insertion loss of the curved barrier stabilises and the difference between the two is always more than 3 dB. From the analysis of Figure 18, it is highlighted that the barrier with porous material has a better performance in comparison with the purely reflective barriers for the whole frequency range under analysis. The performance of the curved barrier with porous material translates into an insertion loss greater than 10 dB in the whole frequency range, reaching 15 dB in a large part of those frequencies and for the frequency of 3150 Hz the insertion loss exceeds 25 dB. In practical terms, for the lowest frequencies (200–630 Hz), the difference between the three barriers under analysis is not more than 2/3 dB between them; however, from 630 Hz on, the performance of the curved barrier with porous material is clearly superior in relation to the other solutions presented.

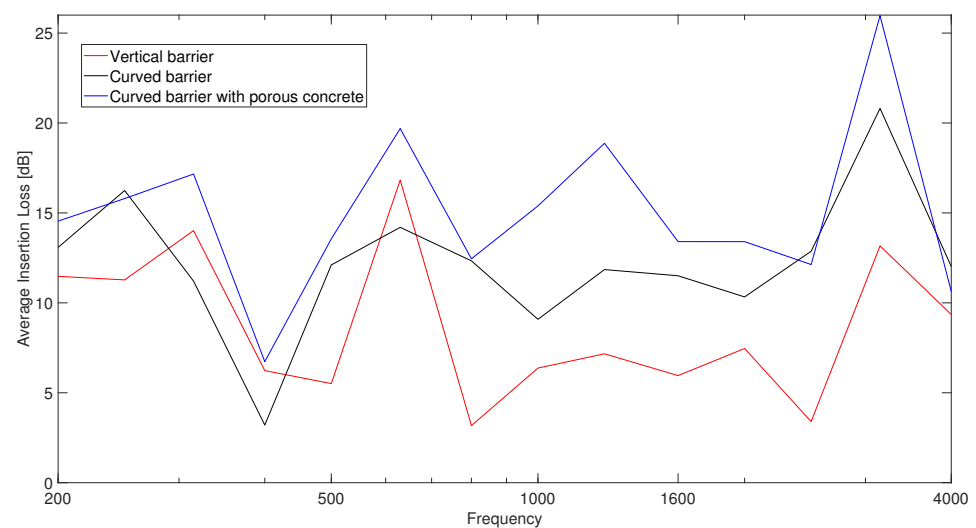


Figure 18. Insertion loss calculated for the three proposed noise barriers.

As observed, the barriers studied have satisfactory levels of insertion loss. Taking into consideration the maximum insertion loss values recorded for the frequencies 630 Hz, 1250 Hz and 3150 Hz, we tried to understand what role the porous material would have, which allowed the mitigation level to be considerably higher at the frequencies mentioned. Figure 19 is divided into three distinct parts: the vertical barrier, Figure 19a–c; curved barrier, Figure 19d–f; and curved barrier with porous material, Figure 19g–i. In Figure 19, the influence of the porous materials on the higher frequencies (1250 Hz and 3150 Hz) is shown, namely in the area between the vehicle and the barrier where the red and yellow colouration is less intense; therefore, less energy is sent to the receivers and there are higher mitigation levels, corroborating the results presented in Figure 18. Regarding the frequency of 630 Hz, as illustrated in Figure 18, the behaviour of the curved barriers in relation to the vertical barrier is not as superior as in the cases of the other frequencies under analysis, partly due to the minor influence of the porous material in controlling reflections between the barrier and the vehicle (Figure 19a,d,g).

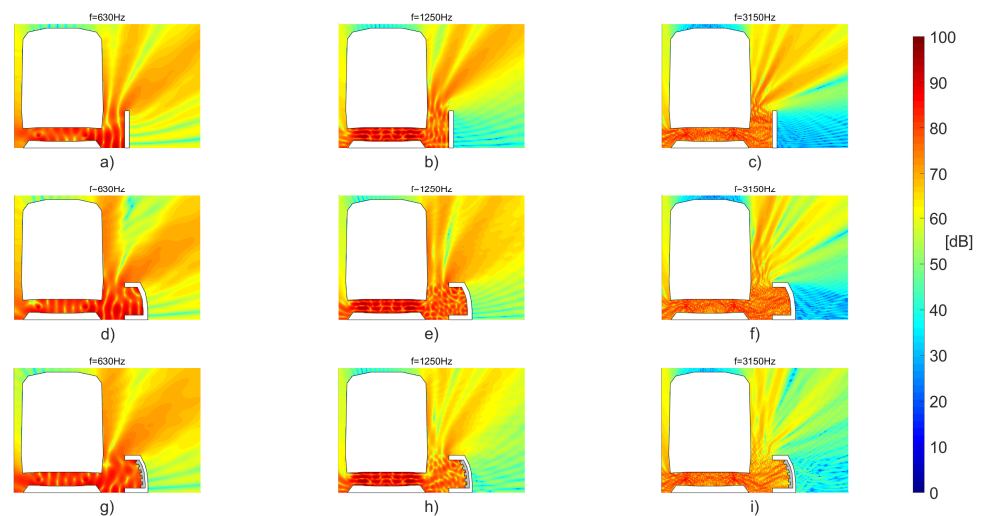


Figure 19. Comparison of the SPL for the vertical barrier (a–c), for the curved barrier (d–f) and for the curved barrier with porous material (g–i)

IL colour maps are plotted for the centre frequencies of the one-third octave bands (315–4000 Hz) in Figures 20 and 21 for the curved barrier scenario with porous material. Through analysing the IL maps, one realises that the influence of the barrier on the more distant receivers is very relevant, namely for the higher frequency bands (Figure 20). It should also be noted that, except for some frequencies, the shadow zone of the barrier increases its influence in height as one moves away from the barrier. According to these results, the receivers placed higher and further away from the barrier still exhibit a good level of protection. Finally, it is possible to observe that for 3150 Hz the shadow zone covers almost the entire receiver array, with IL very close or above 25 dB for all receivers.

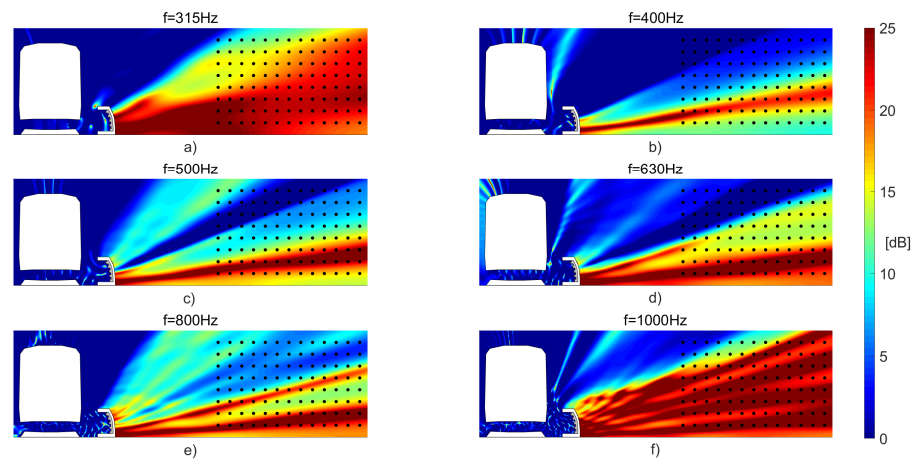


Figure 20. Insertion loss maps for the curved noise barrier with absorptive layer for frequencies 315 Hz, 400 Hz, 500 Hz, 630 Hz, 800 Hz and 1000 Hz (a–f), with the presence of the receivers (black dots) used to calculate mean IL (Figure 18).

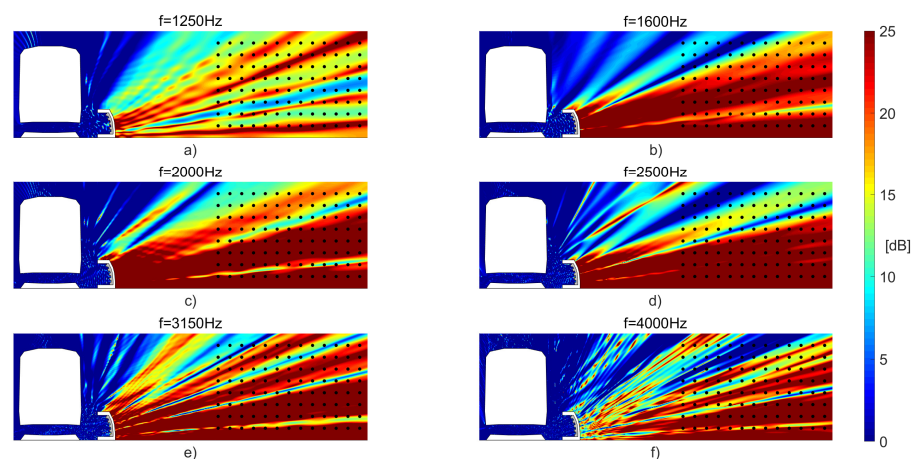


Figure 21. Insertion loss maps for the curved noise barrier with absorptive layer for frequencies 1250 Hz, 1600 Hz, 2000 Hz, 2500 Hz, 3150 Hz and 4000 Hz (a–f), with the presence of the receivers (black dots) used to calculate mean IL (Figure 18).

7. Conclusions

This paper presents the development of a low-height acoustic barrier to be used close to the noise source in a railway environment. The development of the solution is composed by two distinct phases, namely the optimisation of the barrier geometry and the integration of a porous material in order to increase the acoustic performance of the solution. Taking advantage of sound pressure level records acquired in the railway environment in the metropolitan area of Porto, it was possible to define the most important frequency content and thus design a solution whose performance was superior in that frequency range. The numerical modelling and study of the various solutions were carried out by applying a BEM formulation with multiple regions, simulating the porous material as an equivalent fluid and thus incorporating its acoustic absorption properties. The parametric study presents the methodology for sizing the curved barrier. Through the simulation of a sound wave, the inner face of the barrier was constructed so that it coincides with the shape of the incident wave front coming from the source. Thus, the reflection normal to the propagation direction is favoured and, as such, more energy is sent in the direction of the noise source and the railway. In this way, an integrated solution was built taking

advantage of the acoustic absorption capacity of the track to absorb the energy sent back. In a complementary manner, a porous concrete layer was added, which on the one hand has a good acoustic absorption capacity and on the other hand guarantees the durability required for solutions used outdoors. The main purpose of the porous material is to absorb part of the energy arising from the reflections between the barrier and the vehicle, ensuring that the energy that is not sent back to the track can be sent in the direction of the external receivers. The results presented show the clear improvement achieved by using porous material as a means of absorbing part of the energy in detriment of purely reflective solutions. The curved solution with porous material presents an IL in the defined receivers higher than 10 dB in all the calculated frequency range; for some frequencies the IL value is even higher than 15 dB, with the maximum registered in the frequency 3150 Hz where the IL value is higher than 25 dB. In this way, the presented solution appears to be a useful element for the reduction in train-induced noise, guaranteeing an effective mitigation. In addition, due to its low-height, this solution does not represent a visual obstacle, as is usual for noise barriers, but it still effectively reduces noise levels at the receivers of interest.

Author Contributions: Conceptualisation, J.L., M.P., P.A.C. and L.G.; methodology, J.L., M.P., P.A.C. and L.G.; software, J.L., M.P. and L.G.; validation, J.L., M.P., P.A.C. and L.G.; formal analysis, J.L., M.P., P.A.C. and L.G.; investigation, J.L. and M.P.; resources, J.L., M.P., P.A.C. and L.G.; data curation, J.L. and M.P.; writing—original draft preparation, J.L. and M.P.; writing—review and editing, P.A.C. and L.G.; visualisation, J.L., M.P., P.A.C. and L.G.; supervision, P.A.C. and L.G.; project administration, P.A.C. and L.G.; funding acquisition, J.L., P.A.C. and L.G. All authors have read and agreed to the published version of the manuscript.

Funding: This research was funded by Base Funding—UIDB/04708/2020 and Programmatic Funding—UIDP/04708/2020 of the CONSTRUCT—Instituto de I&D em Estruturas e Construções—funded by national funds through the FCT/MCTES (PIDDAC); Base Funding—UIDB/04029/2020—of ISISE (Institute for Sustainability and Innovation in Structural Engineering) funded by national funds through the FCT/MCTES (PIDDAC); Project POCI-01-0247-FEDER-033990 funded by FEDER funds through COMPETE2020—Programa Operacional Competitividade e Internacionalização (POCI); National funds (PIDDAC) through FCT/MCTES; Individual Grant: SFRH/BD/148367/2019.

Conflicts of Interest: The authors declare no conflict of interest.

References

1. EEA (European Environment Agency). *Environmental Noise in Europe—2020*; Technical Report; EEA (European Environment Agency): Copenhagen, Denmark, 2020; ISBN 9789294802057.
2. Blanes, N.; Marin, A.; Ramos, U.M.J. *Noise Exposure Scenarios in 2020 and 2030 Outlooks for EU 28*; Technical Report; European Topic Centre on Air Pollution, Transport, Noise and Industrial Pollution—Norwegian Institute for Air Research: Kjeller, Norway, 2019.
3. World Health Organization. *Environmental Noise Guidelines for the European Region*; World Health Organization: Copenhagen, Denmark, 2018.
4. De Vos, P. *Railway Noise in Europe. State of the Art Report*; International Union of Railways (UIC): Paris, France, 2016.
5. Maffei, L.; Masullo, M.; Aletta, F. Influence of the design of railway noise barriers on soundscape perception. In Proceedings of the INTER-NOISE and NOISE-CON Congress and Conference Proceedings. Institute of Noise Control Engineering, Lexington, KY, USA, 13–15 June 2012; Volume 2012, pp. 1966–1972.
6. European Commission. *Hosanna—Holistic and Sustainable Abatement of Noise by Optimized Combinations of Natural and Artificial Means*; European Commission: Brussels, Belgium, 2009.
7. Crocker, M.J. *Handbook of Noise and Vibration Control*; John Wiley & Sons: Hoboken, NJ, USA, 2007.
8. Thompson, D. *Railway Noise and Vibration: Mechanisms, Modelling and Means of Control*; Elsevier: Amsterdam, The Netherlands, 2008.
9. Koussa, F.; Defrance, J.; Jean, P.; Blanc-Benon, P. Acoustic performance of gabions noise barriers: Numerical and experimental approaches. *Appl. Acoust.* **2013**, *74*, 189–197. [[CrossRef](#)]
10. Jolibois, A.; Defrance, J.; Koreneff, H.; Jean, P.; Duhamel, D.; Sparrow, V.W. In situ measurement of the acoustic performance of a full scale tramway low height noise barrier prototype. *Appl. Acoust.* **2015**, *94*, 57–68. [[CrossRef](#)]
11. Nieuwenhuizen, E.; Yntema, N. The effect of close proximity, low height barriers on railway noise. In Proceedings of the Euronoise, Heraklion, Greece, 27–31 May 2018; pp. 1375–1380.
12. Kasess, C.H.; Kreuzer, W.; Waubke, H. Deriving correction functions to model the efficiency of noise barriers with complex shapes using boundary element simulations. *Appl. Acoust.* **2016**, *102*, 88–99. [[CrossRef](#)]

13. Krezel, Z.A.; McManus, K. Recycled aggregate concrete sound barriers for urban freeways. In *Waste Management Series*; Elsevier: Harrogate, UK, 2000; Volume 1, pp. 884–892.
14. Magrini, U.; Ricciardi, P. Surface sound acoustical absorption properties of multilayer panels. In Proceedings of the INTER-NOISE and NOISE-CON Congress and Conference Proceedings, Nice, France, 27–31 August 2000; Institute of Noise Control Engineering: Reston, VA, USA, 2000; Volume 2000, pp. 2953–2959.
15. Asdrubali, F.; Horoshenkov, K. The acoustic properties of expanded clay granulates. *Build. Acoust.* **2002**, *9*, 85–98. [[CrossRef](#)]
16. Vašina, M.; Hughes, D.; Horoshenkov, K.; Lapčík, L., Jr. The acoustical properties of consolidated expanded clay granulates. *Appl. Acoust.* **2006**, *67*, 787–796. [[CrossRef](#)]
17. Bartolini, R.; Filippozzi, S.; Princi, E.; Schenone, C.; Vicini, S. Acoustic and mechanical properties of expanded clay granulates consolidated by epoxy resin. *Appl. Clay Sci.* **2010**, *48*, 460–465. [[CrossRef](#)]
18. Kim, H.K.; Lee, H.K. Influence of cement flow and aggregate type on the mechanical and acoustic characteristics of porous concrete. *Appl. Acoust.* **2010**, *71*, 607–615. [[CrossRef](#)]
19. San Martín, J.C.; Esquerdo-Lloret, T.V.; Ramis-Soriano, J.; Nadal-Gisbert, A.V.; Denia, F.D. Acoustic properties of porous concrete made from arlite and vermiculite lightweight aggregates. *Cons. Super. Investig. Cient.* **2015**, *65*, e072.
20. Tie, T.S.; Mo, K.H.; Putra, A.; Loo, S.C.; Alengaram, U.J.; Ling, T.C. Sound absorption performance of modified concrete: A review. *J. Build. Eng.* **2020**, *30*, 101219. [[CrossRef](#)]
21. Pereira, A.; Godinho, L.; Morais, L. The acoustic behavior of concrete resonators incorporating absorbing materials. *Noise Control. Eng. J.* **2010**, *58*, 27–34. [[CrossRef](#)]
22. Carbajo, J.; Esquerdo-Lloret, T.V.; Ramis, J.; Nadal-Gisbert, A.V.; Denia, F.D. Acoustic modeling of perforated concrete using the dual porosity theory. *Appl. Acoust.* **2017**, *115*, 150–157. [[CrossRef](#)]
23. Pereira, M.; Carbajo San Martín, J.; Godinho, L.; Amado-Mendes, P.; Mateus, D.; Ramis-Soriano, J. Acoustic behavior of porous concrete. Characterization by experimental and inversion methods. *Inst. Cienc. Constr. Eduardo Torroja* **2019**, *69*, e202. [[CrossRef](#)]
24. Zolanvari, S.M.H. *Numerical Modeling and Material Development of a Concrete-Based Acoustic Absorber*; Fraunhofer Verlag: Stuttgart, Germany, 2019.
25. Kirkup, S.M. *The Boundary Element Method in Acoustics*; Integrated Sound Software; University of Central Lancashire: Preston, UK, 2007.
26. Hemsworth, B. Environmental noise directive development of action plans for railways. In *UIC Noise Expert Network: International Union of Railways (UIC)*; Union Internationale des Chemins de fer (UIC): Paris, France, 2008.
27. Berzborn, M.; Bomhardt, R.; Klein, J.; Richter, J.G.; Vorländer, M. The ITA-Toolbox: An open source MATLAB toolbox for acoustic measurements and signal processing. In Proceedings of the 43th Annual German Congress on Acoustics, Kiel, Germany, 6–9 March 2017; Volume 2017, pp. 6–9.
28. Ciaburro, G.; Iannace, G.; Ali, M.; Alabdulkarem, A.; Nuhait, A. An artificial neural network approach to modelling absorbent asphalts acoustic properties. *J. King Saud-Univ. Eng. Sci.* **2021**, *33*, 213–220. [[CrossRef](#)]
29. Arenas, J.P.; Rebolledo, J. Acoustic characterization of loose-fill cellulose crumbs obtained from wood fibers for sound absorption. In Proceedings of the INTER-NOISE and NOISE-CON Congress and Conference Proceedings, Innsbruck, Austria, 15–18 September 2013; Austrian Noise Abatement Association Austrian Noise Abatement Association: Vienna, Austria; Institute of Noise Control Engineering: Reston, VA, USA, 2013; Volume 247, pp. 1734–1739.
30. del Rey, R.; Bertó, L.; Alba, J.; Arenas, J.P. Acoustic characterization of recycled textile materials used as core elements in noise barriers. *Noise Control. Eng. J.* **2015**, *63*, 439–447. [[CrossRef](#)]
31. ISO. *Acoustics—Determination of Sound Absorption Coefficient and Impedance in Impedance Tubes—Part 2: Transfer-Function Method*; Technical Report; International Organization for Standardization: Geneva, Switzerland, 1998.
32. Utsuno, H.; Tanaka, T.; Fujikawa, T.; Seybert, A. Transfer function method for measuring characteristic impedance and propagation constant of porous materials. *J. Acoust. Soc. Am.* **1989**, *86*, 637–643. [[CrossRef](#)]
33. Horoshenkov, K.V.; Swift, M. The acoustic properties of granular materials with pore size distribution close to log-normal. *J. Acoust. Soc. Am.* **2001**, *110*, 2371–2378. [[CrossRef](#)] [[PubMed](#)]
34. Pereira, M.; Carbajo, J.; Godinho, L.; Ramis, J.; Amado-Mendes, P. Improving the sound absorption behaviour of porous concrete using embedded resonant structures. *J. Build. Eng.* **2020**, *35*, 102015. [[CrossRef](#)]
35. Marburg, S.; Nolte, B. *Computational Acoustics of Noise Propagation in Fluids: Finite and Boundary Element Methods*; Springer: Berlin/Heidelberg, Germany, 2008; Volume 578.
36. Chandler-Wilde, S.; Langdon, S. *Boundary Element Methods for Acoustics*; Lecture Notes; Department of Mathematics, University of Reading: Berkshire, UK, 2007.
37. Seybert, A.; Cheng, C.; Wu, T. The solution of coupled interior/exterior acoustic problems using the boundary element method. *J. Acoust. Soc. Am.* **1990**, *88*, 1612–1618. [[CrossRef](#)]
38. Broadbent, R.; Thompson, D.; Jones, C. The acoustic properties of railway ballast. In Proceedings of the Euronoise 2009, Edinburgh, UK, 26–28 October 2009.